X-band AlGaN/GaN HEMT MMIC Voltage-Controlled Oscillator

Val Kaper[1], Richard Thompson[1], Tom Prunty[1], James R. Shealy[1]

[1]Cornell University, School of Electrical and Computer Engineering, 112 Phillips Hall, Ithaca NY 14853, USA
1-607-257-3257, kaperv@ece.cornell.edu

***Abstract*— A monolithic AlGaN/GaN HEMT voltage-controlled oscillator has been designed, fabricated and characterized. The oscillator design utilizes a common-gate negative resistance topology with a multi-finger interdigitated Schottky diode varactor resonator for frequency control. The VCO operating at 15 V drain bias and -4 V gate bias, exhibits frequency range between 8.5 and 9.5 GHz with maximum output power of 31.8 dBm across a 50 ohm load. Maximum power variation does not exceed $\pm$ 0.8 dB in the oscillation frequency band. Average phase noise in the bandwith is estimated to be equal to -77 dBc/Hz at 100 kHz offset and -101 dBc/Hz at 1 MHz offset. Average tuning sensitivity is measured to be 120 MHz/V. Oscillator's pulling figure is equal to 139 MHz for 12 dB return loss. Pushing figure is 114 MHz/V. Output power can be increased up to 35 dBm (2.1 W/mm) by setting drain bias voltage at 30 V.**

I. Introduction

Aluminum Gallium Nitride / Gallium Nitride high electron mobility transistors (AlGaN/GaN HEMT's) is a new technology for high power applications at RF, microwave and millimeter-wave frequencies. Due to its unique physical properties, most importantly high critical electrical field and high sheet charge concentration, these devices are capable of generating, amplifying and delivering signals with power levels an order of magnitude larger than GaAs-based transistors. Initial research has been focused on demonstrating the viability of this technology for high-power broadband amplifiers [1], [2]. The same unique physical properties has been exploited to implement a high-power fixed frequency oscillator [3]. Absence of intentional ionized impurities in the material structure, which may act as a noise source, have allowed for the demonstration of a low-phase noise hybrid VCO [4].

In this paper we present the first, to authors' knowledge, implementation of a fully monolithic X-band AlGaN/GaN HEMT VCO.

II. Epitaxial Growth and Device Fabrication

Epitaxial layers for the AlGaN/GaN HEMT structure are grown by organo-metallic vapor phase epitaxy (OMVPE). First, an AlGaN nucleation layer is grown on the (0001) surface of a semi-insulating SiC substrate followed by an AlN(2000Å) [5] layer. Then, a 1 μm thick GaN buffer layer is deposited. Finally, a composite barrier is grown, consisting of a 15 Å AlN interlayer, a 200 Å thick layer of undoped $Al_{0.35}Ga_{0.65}N$ and a 20 Å GaN cap. Discontinuity of spontaneous and piezoelectric polarization vectors across the heterointerface (AlGaN/AlN/GaN) induces two-dimensional electron gas (2-DEG) at the interface. The AlN interlayer improves electron mobility by reducing alloy related scattering at the heterointerface [6]. The GaN cap raises Schottky barrier height and reduces gate leakage. It has also been observed [7] that the GaN cap helps to minimize current collapse and increases off-state breakdown voltage. C-V and Hall measurements of the grown structure show existence of a sheet charge with concentration of 1.7 x 10^{13} cm^{-2} and typical room temperature mobility of 1200 $cm^2/(V*s)$.

Device fabrication on grown epitaxial layers starts with the deposition of Ti/Pt alignment marks for e-beam- and photolithographies. Mesa isolation is then photolithographically patterned and etched with chlorine-based ECR plasma.

Ti(20 nm)/Al(100 nm)/Ti(45 nm)/Au(55 nm) ohmic contacts are patterned with e-beam lithography, deposited with e-gun evaporation and annealed at 800°C for 60 seconds. Ohmic contact resistance and sheet resistance, measured using TLM method, were equal to 0.5 ohm-mm and 280 ohm/square respectively. Ni(25 nm)/Au(375 nm) mushroom gates were written with an e-beam, developed using the triple resist stack of PMMA/Copolymer/PMMA and deposited with e-gun evaporation. The first interconnect level is defined by photolithography and uses deposition of 3500 Å of Au to form the contact pads. Preliminary device characterization is then performed. Following that, an 1800 Å thick PECVD Si_3N_4 film is deposited in order to passivate the surface [8] as well as to form the insulator layer for MIM capacitors. The second interconnect level processing, which consists of via hole etching, airbridge post definitions and deposition, seed layer evaporation and electrochemical plating of 3 μm thick Au, concludes the device fabrication sequence. A more detailed description of the epitaxial growth and device fabrication can be found in [5] and [9].

Device parameters of a fabricated 0.15 μm x 200 μm HEMT are: open-channel current density (I_{max}) = 1300 mA/mm, peak transconductance (g_{mmax}) = 350 mS/mm, pinch-off voltage (V_{po}) = -4.2 V, current gain cutoff frequency (f_t) = 60 GHz, maximum oscillation frequency (f_{max}) = 50 GHz, maximum output power densities (P_{out}) at 10 GHz are 2.6 W/mm (V_{ds} = 15 V), 6.6 W/mm (V_{ds} = 30 V), 10 W/mm (V_{ds} = 50 V - maximum sustainable drain bias voltage).

III. VCO Design

The oscillator design is based on a common-gate AlGaN/GaN HEMT with 0.15 μm gate length and 1.5 mm total gate width (10 fingers). Inductive feedback connected to the HEMT's gate electrode in conjunction with the output matching network connected to the drain electrode were designed to maximize input negative resistance, i.e. transistor instability. HEMT's input inductive impedance is resonated with a capacitive impedance of a combination of a 10-finger interdigitated Schottky diode varactor, a series MIM capacitor

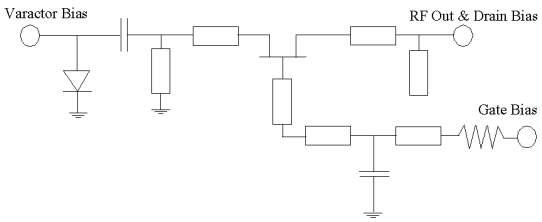

Fig. 1. AlGaN/GaN HEMT VCO Schematic.

and a short-circuit stub, connected to the HEMT's source electrode.

To obtain required range of capacitances between 0.6 pF and 6 pF, the varactor was fabricated with 1 μm rectangular gate and 1.5 mm gate width, based on previously extracted value of the capacitance per unit width of 4 pF/mm for this gate length. Large total gate width of the varactor allows to minimize gate and access resistances, and thus ensures that the resonator resistance stays much less than the magnitude of the negative resistance generated by the unstabilized HEMT, which is a necessary condition for oscillation start-up. It also increases the Q-factor of the varactor, which directly affects the phase noise of the oscillator. The purpose of the series MIM capacitor is to uncouple the varactor control voltage and the DC grounded HEMT's source electrode. The length of the short-circuit stub was designed to have large enough impedance in the expected VCO bandwidth so that it will not affect overall resonator impedance.

The oscillator requires positive drain and negative gate bias. Varactor capacitance is controlled by the negative control voltage. All transmission lines are implemented with coplanar waveguide transmission lines. Inductive feedback is implemented with a high impedance (Z_0 = 80 ohm) transmission line. The source short-circuit stub and a transmission line connecting the transistor drain with the circuit's RF output pad are implemented with an airbridge transmission line (Z_0 = 68 ohm) with larger current handling limit in order to prevent possible electromigration problems that may arise due to significant expected value for Ids $\approx$ 500 mA. The open-circuit stub in the output matching network uses low impedance (Z0 = 35 ohm) line to minimize its length. Gate DC bias is provided through a bulk resistor and a shunt MIM capacitor. The final circuit schematic is depicted in Fig. 1

Initial circuit design was performed with a linear simulation using measured small-signal S-parameters of a discrete HEMT and bias-dependent S-parameters of a Schottky diode. Particular attention has been paid to select HEMT and Schottky diode gate length and width such that the varactor's capacitive impedance will resonate with HEMT's input inductive impedance, while the oscillation start-up condition is satisfied. Simulated real and imaginary parts of the input and resonator impedances are shown in Figs. 2 and 3. At lower oscillation frequency negative resistance R_{neg} and resonator resistance R_{res} are -92 ohm and 9 ohm respectively, at upper oscillation frequency they are -16 ohm and 2 ohm respectively. Thus, in both cases as well as at all intermediate control voltages, the oscillation start-up condition is satisfied. A large-signal simulation with a nonlinear Statz FET model has been used to verify linear simulation results and to predict power at fundamental and harmonic frequencies as well as DC power consumption.

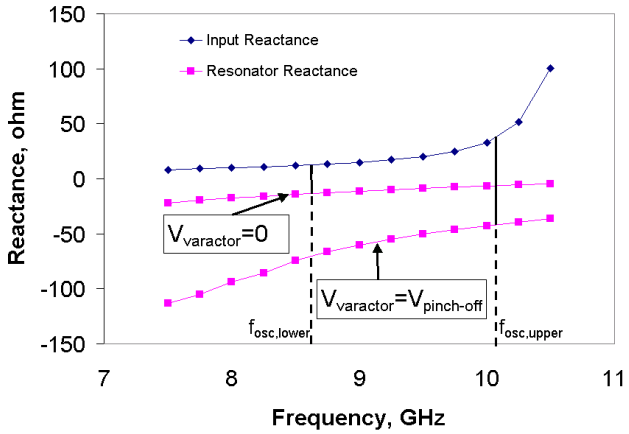

Fig. 2. Linear simulation: oscillation may occur at frequency at which sum of input and resonator reactances is zero.

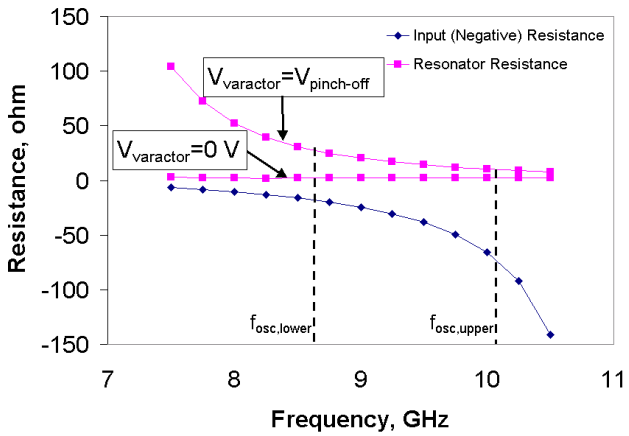

Fig. 3. Linear simulation: input(negative) and resonator resistances are satisfying oscillation start-up conditions $|R_{res}| \leq |R_{neg}/3|$.

IV. Experimental Results

An SEM image of the fabricated circuit is shown in Fig. 4. VCO layout occupies an area of 1.6 mm^2.

The voltage-controlled oscillator has been characterized on-wafer with an Agilent8562A Spectrum Analyzer. Dependence of the oscillation frequency and output power on varactor bias is shown in Fig. 5. At 15 V drain bias, the oscillator exhibits 1 GHz (>10%) bandwith with 9 GHz center frequency. Measured VCO's maximum output power is 31.8 dBm. Output power variation in the frequency band does not exceed $\pm$ 0.8 dB with average power of 31.1 dBm. DC-RF efficiency varies between 17% and 21%. Measured output power and DC-RF efficiency show reasonable correlation with large-signal simulation. The difference between measured and simulated output power is within 1.5 dB and the difference in the efficiency is less than 5% points. The minimum second and third harmonic suppressions are 21 and 27 dBc respectively. Average tuning sensitivity across the band is 120 MHz/V.

The average phase noise across the bandwith estimated using spectrum analyzer is -77 dBc/Hz at 100 kHz offset and -101 dBc/Hz at 1 MHz offset. As expected, the VCO phase noise value is considerably worse ($\approx$10 dBc/Hz) than for a similar AlGaN/GaN HEMT fixed frequency oscillator [3] with

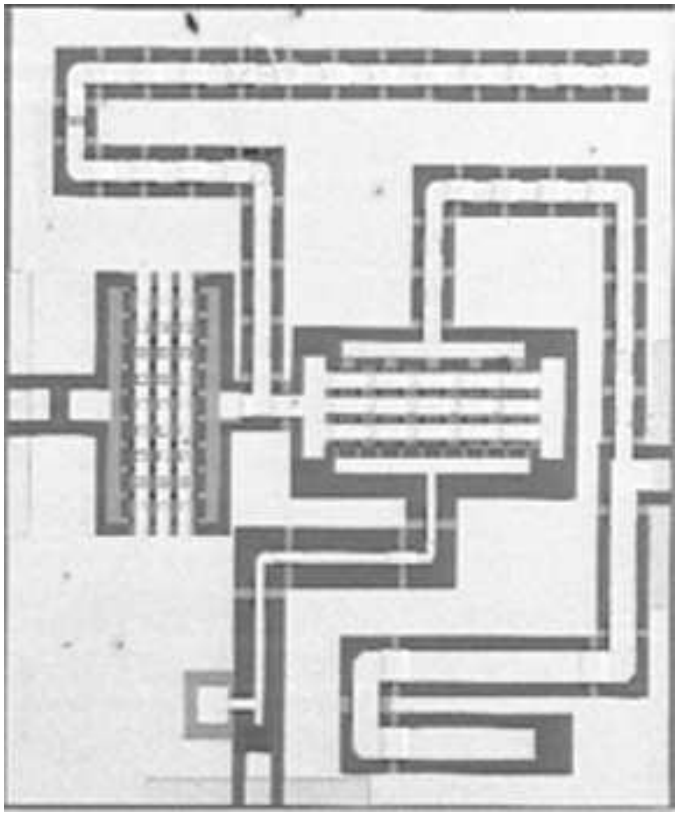

Fig. 4. SEM image of the fabricated AlGaN/GaN HEMT voltage-controlled oscillator.

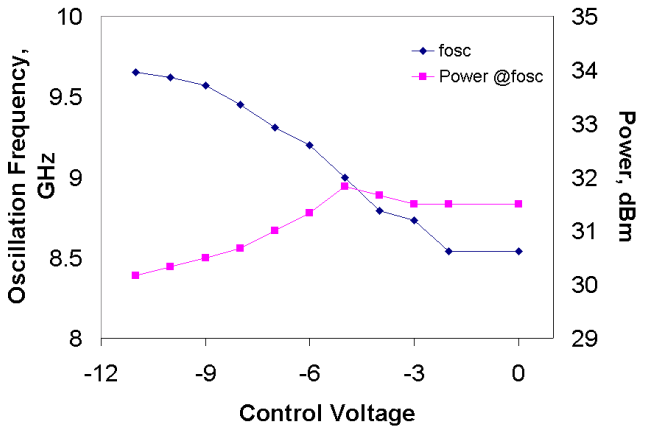

Fig. 5. Measured oscillation frequency and corresponding output power of the AlGaN/GaN HEMT VCO. V_{ds}=15 V, V_{gs}=-4 V.

a transmission line resonator, which has significantly better Q-factor than the Schottky diode varactor. Another VCO figure of merit, which is closely related to phase noise is pushing figure. The pushing figure describes oscillation frequency sensitivity on DC power supply variation, relating inadvertent noise in DC bias line to unwanted sideband noise. For the presented circuit the pushing figure was measured to be equal to 114 MHz/V. Dependence of the oscillation frequency on gate bias is depicted in Fig.6.

Since AlGaN/GaN HEMT stand-alone oscillators can potentially satisfy some system's power requirements without a need for a buffer amplifier, it is important to ensure that the frequency of oscillation will not be overly dependent

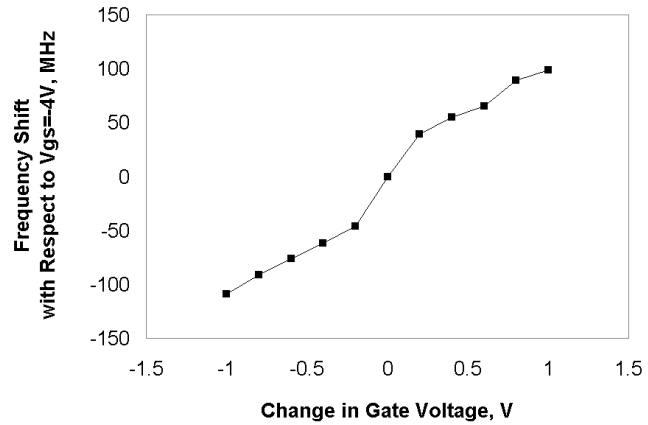

Fig. 6. Pushing figure measurement of the AlGaN/GaN HEMT VCO.V_{ds}=15 V, $V_{varactor}$=0 V.

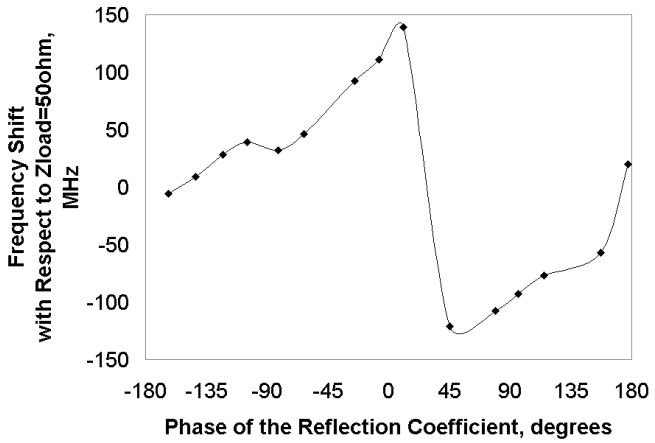

Fig. 7. Pulling figure measurement of the AlGaN/GaN HEMT VCO. V_{ds}=15 V, V_{gs}=-4 V, $V_{varactor}$=0 V.

on variations in external load impedance. The oscillation frequency dependence on load mismatch is shown in Fig. 7. Pulling figure, which signifies the maximum frequency shift for a given change in the load reflection coefficient, was measured to be equal to 139 MHz for a 12 dB return loss mismatch. The pulling figure can be significantly improved at the expense of output power by inserting a passive attenuator on the VCO's output.

Output power can be considerably raised by increasing the drain bias voltage. Dependence of output power and DC-RF efficiency on the drain bias voltage is illustrated in Fig. 8. However, the power increase is accompanied by an increase in the phase noise (≈10 dBc/Hz). Also, as shown in Fig. 8, a slight decrease (≈3% points) in DC-RF efficiency has also been observed.

V. Conclusion

An implementation of a fully monolithic X-band multi-watt voltage control oscillator (VCO) based on AlGaN/GaN high electron mobility transistor (HEMT) is presented. Oscillator bandwith is 1 GHz with a 9 GHz center frequency. Maximum output power measured across 50 ohm load is 31.8 dBm and 35 dBm at 15 V and 30 V drain biases respectively. Power performance of the presented oscillator measures up favorably against comparable GaAs circuits [10], [11]. High

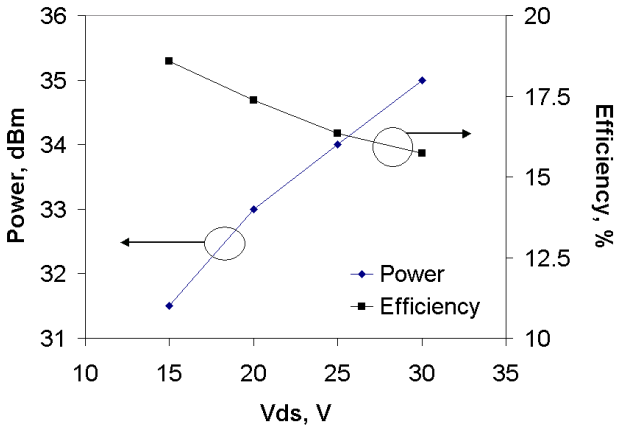

Fig. 8. Output power and DC-RF efficiency increases with drain bias voltage. V_{gs}=-4 V, $V_{varactor}$=0 V.

output power and reasonable pulling figure indicates potential for AlGaN/GaN HEMT oscillators to be used without buffer amplifiers, and thus reduce systems' cost and size.

ACKNOWLEDGEMENT

Authors would like to thank Prof.L.F.Eastman for useful discussions and for access to microwave measurement equipment. Partial support for this work has been provided by Raytheon Company, Northrop Grumman Corporation, Lockheed Martin Corporation and Welch Allyn. This work was performed in part at the Cornell NanoScale Facility (a member of the National Nanofabrication Users Network) which is supported by the National Science Foundation, its users, Cornell University and Industrial Affiliates.

REFERENCES

[1] B. M.Green, V. Tilak, S. Lee, H. Kim, J. A.Smart, K. J.Webb, J. R.Shealy, L. F.Eastman, "High-power broad-band AlGaN/GaN HEMT MMICs on SiC substrates," *IEEE Transactions on Microwave Theory and Techniques*, vol. 49, no. 12, December 2001.

[2] J. J. Xu, S. Keller, G. Parish, S. Heikman, U. K.Mishra, R. A.York,"A 3-10-GHz GaN-based flip-chip integrated broad-band power amplifier," *IEEE Transactions on Microwave Theory and Techniques*, vol. 48, no. 12, December 2000.

[3] V. Kaper, V. Tilak, H. Kim, R. Thompson, T. Prunty, L. F.Eastman, J. R.Shealy,"High Power Monolithic AlGaN/GaN HEMT Oscillator," *Digest of Gallium Arsenide Integrated Circuit (GaAs IC) Symposium*, October 2002.

[4] J. B.Shealy, J. A.Smart, J. R.Shealy,"Low-phase noise AlGaN/GaN FET-based voltage controlled oscillators (VCOs)," *IEEE Microwave and Wireless Components Letters*, Vol.11, no. 6, June 2001.

[5] J. R.Shealy, V. Kaper, V. Tilak, T. Prunty, J. A.Smart, B. Green, L. F.Eastman, "An AlGaN/GaN high-electron-mobility transistor with an AlN sub-buffer layer," *Journal of Physics: Condensed Matter*, vol. 14, April 2002.

[6] L. Shen, S. Heikman, B. Moran, R. Coffe, N. -Q.Zhang, D. Buttari, I. P.Smorchkova, S. Keller, S. P.DenBaars, U. K.Mishra, "AlGaN/AlN/GaN High Power Microwave HEMT," *IEEE Electron Device Letters*, vol. 22, no. 10, October 2001.

[7] T. Kikkawa, M. Nagahara, T. Kimura, S. Yokokawa, S. Kato, M. Yokoyama, Y. Tateno, K. Horino, K. Domen, Y. Yamaguchi, N. Hara, and K. Joshin, "A 36 W CW AlGaN/GaN-Power HEMT Using Surface-Charge-Controlled Structure," *2002 MTT-s Digest*, June 2002.

[8] B. M.Green, K. K.Chu, E. M. Chumbes, J. A.Smart, J. R. healy, L. F.Eastman, "The effect of surface passivation on the microwave characteristics of undoped AlGaN/GaN HEMT's," *IEEE Electron Device Letters*, Vol.21, no. 6, June 2000.

[9] L. F.Eastman, V. Tilak, J. Smart, B. M.Green, E. M.Chumbes, R. Dimitrov, Hyungtak Kim, O. Ambacher, N. Weimann, T. Prunty, M. Murphy, W. J.Schaff, J. R.Shealy, "Undoped AlGaN/GaN HEMTs for Microwave Power Amplification," *IEEE Transactions on Electron Devices*, March 2001.

[10] A. W.Dearn, "MMIC Oscillator Design," *IEE Colloquium on MMIC's Digest*, pp.8/1-8/6, November 1995.

[11] C. -H.Lee, S. Han, B. Matinpour, J. Laskar, "A low phase noise X-band MMIC GaAs MESFET VCO,"*IEEE Microwave and Wireless Components Letters*, Vol.10 no. 6, pp.325-327, August 2000.